MULTI-TARGET DETECTION WITH THE GENERALIZED METHOD OF MOMENTS

Ye'Ela Shalit, Ran Weber*, Asaf Abas*, Shay Kreymer*, and Tamir Bendory*

School of Electrical Engineering, Tel Aviv University, Tel Aviv, Israel

ABSTRACT

The abstract should appear at the top of the left-hand column of text, about 0.5 inch (12 mm) below the title area and no more than 3.125 inches (80 mm) in length. Leave a 0.5 inch (12 mm) space between the end of the abstract and the beginning of the main text. The abstract should contain about 100 to 150 words, and should be identical to the abstract text submitted electronically along with the paper cover sheet. All manuscripts must be in English, printed in black ink.

***Index Terms*—** One, two, three, four, five

1. INTRODUCTION

We study the multi-target detection (MTD) problem of estimating a target signal $x \in \mathbb{R}^L$ from a noisy measurement that contains multiple copies of the signal, each randomly translated [1], [2], [3], [4], [5], [6]. Specifically, let $x \in \mathbb{R}^L$ be a measurement of the form

$$y[\ell] = \sum_{i=1}^{p} x[\ell - \ell_i] + \varepsilon[\ell], \tag{1}$$

where $\{\ell_i\}_{i=1}^p \in \{L+1, \dots, N-L\}$ are arbitrary translations, and $\varepsilon[\ell]$ is i.i.d. Gaussian noise with zero mean and variance σ^2.

The translations and the number of occurrences of x in y are unknown. Figure 1 presents an example of a measurement y at different signal-to-noise ratios (SNRs). We define SNR $:= \frac{\|x\|_2^2}{L\sigma^2}$, where L is the length of x (in pixels), and σ^2 is the noise variance.

The MTD model arises in several scientific applications, such as passive radar [7], astronomy [8], motion deblurring [9], and system identification [10]. In particular, it serves as mathematical abstraction of the cryo-electron microscopy (cryo-EM) technology for macromolecular structure determination [11], [12], [13]. In a cryo-EM experiment [14], biological macromolecules suspended in a liquid solution are rapidly frozen into a thin ice layer. An electron beam then passes through the sample, and a two-dimensional tomographic projection is recorded. Importantly, the 2-D location and 3-D orientation of particles within the ice are random and unknown. This measurement, called *micrograph*, is affected by high noise levels and the optical configuration of the microscope. This transformation is typically modeled as a convolution of the model (1) with a point spread function, whose Fourier transform is called contrast transfer function (CTF) [15], [16].

In the current analysis workflow of cryo-EM data [17], [18], [19], the 2-D projections are first detected and extracted from the micrograph, and later rotationally and translationally aligned to reconstruct the 3-D molecular structure. This approach fails for small molecules, which induce low contrast, and thus low SNR. This makes them difficult to detect and align [6], [11], [17], [20], rendering current cryo-EM algorithmic pipeline ineffective. For example, in the limit SNR $\to 0$, reliable detection of signals' locations within the measurement is impossible [6, Proposition 3.1].

The MTD model was devised in [6] in order to study the recovery of small molecules directly from the micrograph, below the current detection limit of cryo-EM [11], [21]. An autocorrelation analysis technique (see Section 2.1) was implemented to recover low-resolution 3-D structures from noiseless simulated data under a simplified model. Autocorrelation analysis consists of finding an image that best explains the empirical autocorrelations of the measurement, by minimizing a least-squares (LS) objective. For any noise level, those autocorrelations can be estimated to any desired accuracy for sufficiently large N. Computing the autocorrelations is straightforward and requires only one pass over the data, which is advantageous for massively large datasets, such as cryo-EM datasets [17]. As such, autocorrelation analysis provides an attractive alternative to other computational methods, such as maximum likelihood estimation, which is intractable for the MTD problem [2].

Autocorrelations analysis is an variation of the method of moment (MoM), which is a classical statistical inference technique, tracing back to 1894 [22]. This work studies the application of the estimator *generalized method of moments* (GMM) and its application to the MTD problem. The GMM theory, which was first introduced in [23], shows that the GMM provides an optimal estimator, in compare to others weighted LS objective function. As shown in previous work, the GMM estimator suggests a significant improvement in the estimation error [23, 24, 25, 26].

* These four authors have contributed equally to this work.

S.K. is supported by the Yitzhak and Chaya Weinstein Research Institute for Signal Processing. T.B. is supported in part by NSF-BSF grant no. 2019752, and the Zimin Institute for Engineering Solutions Advancing Better Lives.

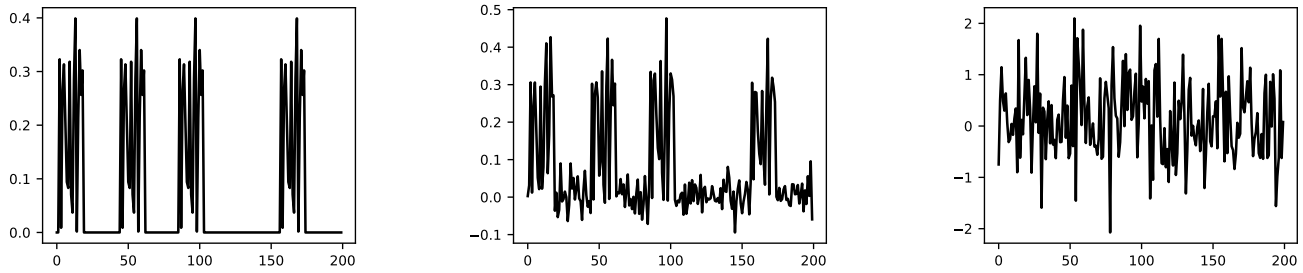

(a) No noise. (b) SNR $= 50$. (c) SNR $= 0.1$.

Fig. 1: Three measurements y from (1) at different noise levels: no noise (left); SNR $= 50$ (middle); SNR $= 0.1$ (right). Each measurement contains multiple copies of the target signal in arbitrary locations. In this work, our goal is to estimate the target signal directly from y. We focus on the low SNR regime (e.g., panel (c)) in which the signal occurrences are swamped by the noise, and the locations of the signal occurrences cannot be detected reliably.

2. MATHEMATICAL FRAMEWORK

2.1. Autocorrelation analysis

The autocorrelation of order q of a signal $z \in \mathbb{R}^N$ is defined as

$$A_z^q[\ell_1, \ldots, \ell_{q-1}] := \mathbb{E}_z\Big[\frac{1}{N^2}\sum_{i\in\mathbb{R}^2} z[i]z[i+\ell_1]\cdots z[i+\ell_{q-1}]\Big], \tag{2}$$

[Asaf: Why N^2?]where $\ell_1, \ldots, \ell_{q-1}$ are integer shifts. Indexing out of bounds is zero-padded, that is, $z[i] = 0$ out of the range $\{0, \ldots, N-1\}$. In this work, we use the first three autocorrelations which are explicitly given by

$$A_z^1 = \mathbb{E}_z\left[\frac{1}{N}\sum_{i\in\mathbb{Z}} z\left[i\right]\right], \tag{3}$$

$$A_z^2\left[\ell\right] = \mathbb{E}_z\left[\frac{1}{N}\sum_{i\in\mathbb{Z}} z\left[i\right] z\left[i+\ell\right]\right], \tag{4}$$

$$A_z^3\left[\ell_1, \ell_2\right] = \mathbb{E}_z\left[\frac{1}{N}\sum_{i\in\mathbb{Z}} z\left[i\right] z\left[i+\ell_1\right] z\left[i+\ell_2\right]\right]. \tag{5}$$

As N grows indefinitely, the empirical autocorrelations of z almost surely (a.s.) converge to the population autocorrelations of z:

$$\lim_{N\to\infty}\frac{1}{N}\sum_{i\in\mathbb{Z}^2} z[i]z[i+\ell_1]\cdots z[i+\ell_{q-1}] \overset{\text{a.s.}}{=} A_z^q[\ell_1, \ldots, \ell_{q-1}]. \tag{6}$$

Our goal is to relate the autocorrelations of the measurement with the target signal x. In particular, the first-order autocorrelation is defined as

$$A_y^1 := \frac{1}{N}\sum_{i\in\mathbb{Z}} y[i]. \tag{7}$$

This is the mean of the measurement. The second-order autocorrelation of y, $A_y^2 : \mathbb{Z} \to \mathbb{R}$, is defined by

$$A_y^2[\ell_1] := \frac{1}{N}\sum_{i\in\mathbb{Z}} y[i]y[i+\ell_1], \tag{8}$$

and the third-order autocorrelation $A_y^3 : \mathbb{Z}\times\mathbb{Z} \to \mathbb{R}$ by

$$A_y^3[\ell_1, \ell_2] := \frac{1}{N}\sum_{i\in\mathbb{Z}} y[i]y[i+\ell_1]y[i+\ell_2]. \tag{9}$$

2.2. Autocorrelations under the well-separated model

We first discuss the well-separated case of the MTD problem, which was studied in [1]. In this case, we assume that each signal in the measurement y is separated by at least a full signal length from its neighbors. Specifically, we assume that

$$|\ell_{i_1} - \ell_{i_2}| \geq 2L - 1, \quad \text{for all } i_1 \neq i_2. \tag{10}$$

To compute the third-order autocorrelation (9), we compute the product of y with its two shifts. Importantly, for ℓ-s in the range

$$\mathcal{L} = \{0, \ldots, L-1\}, \tag{11}$$

any given occurrence of x in y is only ever correlated with itself, and never with another occurrence.

In [1], it was shown that under the separation condition (10), for any fixed level of noise σ^2, density γ and signal length L, in the limit $N \to \infty$ we have that

$$A_y^1 \overset{\text{a.s.}}{=} \gamma A_x^1, \tag{12}$$

$$A_y^2[\ell_1] \overset{\text{a.s.}}{=} \gamma A_x^2[\ell_1] + \sigma^2\delta[\ell_1], \tag{13}$$

$$A_y^3[\ell_1, \ell_2] \overset{\text{a.s.}}{=} \gamma A_X[\ell_1, \ell_2] + \gamma S_1\sigma^2(\delta[\ell_1] + \delta[\ell_2] + \delta[\ell_1 - \ell_2]), \tag{14}$$

[Asaf: What is S_1 above?] for $\ell_1, \ell_2 \in \mathcal{L}$ (defined in (11)), where

$$\delta[\ell] = \begin{cases} 1 \text{ if } \ell = \vec{0}, \\ 0 \text{ otherwise}, \end{cases} \tag{15}$$

is the Kronecker delta function. Here, γ is the density of the target images in the measurement and is defined by

$$\gamma = p\frac{L}{N}. \tag{16}$$

Next, we introduce the notations for the second and third autocorrelations:

$$\begin{aligned} \mathcal{A}_y^2 &:= [A_y^2[\ell]]_{\ell=0}^{L-1}, \\ \mathcal{A}_x^2 &:= [A_x^2[\ell] + \sigma^2\delta[\ell]]_{\ell=0}^{L-1}, \\ \mathcal{A}_y^3 &:= [A_y^3[\ell_1, \ell_2]]_{\ell_1,\ell_2=0}^{L-1}, \\ \mathcal{A}_x^3 &:= [A_x^3[\ell_1, \ell_2] + \gamma S_1\sigma^2(\delta[\ell_1] + \delta[\ell_2] + \delta[\ell_1 - \ell_2])]_{\ell_1,\ell_2=0}^{L-1} \end{aligned}$$

Notice, $\mathcal{A}_y^3$ and $\mathcal{A}_x^3$ are treated as vectors.

[Asaf: I'm not sure that this is relevant. We should only mention that 3 auto' are enough in order to recover x and γ]As such, (12) - (14) relate the autocorrelations of the measurement with those of the target signal x. Moreover, the signal x can be identified from its autocorrelations, and thus, potentially, also from the autocorrelations of the measurement. In [1], it was shown that γ (respectively σ) can be estimated from the first- and second-order autocorrelations of the measurement if σ (respectively γ) is known. In particular, if γ and σ are known (or are reliably estimated), we can provably determine the signal from the measurement's autocorrelations. Previous works [1], [2], [3], [4], [5] demonstrated successful signal and image estimations. Importantly, the aforementioned relations between the autocorrelations of M and F do not directly depend on the location of individual signal occurrences in the measurement, but only through the density parameter γ. Therefore, detecting the signal occurrences is not a prerequisite for signal recovery, and thus signal recovery is possible even in very low SNR regimes.

2.3. Signal recovery from autocorrelations

In previous work [1], in order to recover the signal they applied this LS estimator:

$$\begin{aligned} x_{LS}, \gamma_{LS} = \min_{x\in\mathbb{R}^L \gamma\in[0,1]} & w_1(A_y^1 - \gamma A_x^1)^2 + \\ & w_2 \left\|\mathcal{A}_y^2 - \mathcal{A}_x^2\right\|_{fro} + w_3 \left\|\mathcal{A}_y^3 - \mathcal{A}_x^3\right\|_{fro}. \end{aligned} \tag{17}$$

Here, $w_1 = \frac{1}{2}, w_2 = \frac{1}{2n_2}$ and $w_3 = \frac{1}{2n_3}$, where n2, n3 are the number of coefficients used for each autocorrelation order: $n_2 = L - 1, n_3 = \frac{(L-1)(L-2)}{2}$ [27]. This LS estimator (17) represent the base-benchmark for the GMM estimator.

3. GENERALIZED METHOD OF MOMENTS

3.1. The GMM framework

In its most simplified form, the GMM generalizes (17) by replacing the LS objective with a specific optimal weights. This choice guarantees favorable asymptotic statistical properties, such as the minimal asymptotic variance of the estimation error.

Let us define the *moment function*, $f(\theta, y)\colon \Theta \times \mathbb{R}^r \to \mathbb{R}^q$. The moment function needs to be chosen such that its expectation value is zero only at a single point $\theta = \theta_0$. Namely,

$$\mathbb{E}\left[f(\theta, y)\right] = 0 \quad \text{if and only if} \quad \theta = \theta_0. \tag{18}$$

We refer to (18) as the *uniqueness of the parameter set* condition. The moment function must satisfy the uniqueness condition and a few additional regularity conditions (which can be found in [23, 24]). This flexibility enables the GMM to be applied to a wide range of problems, such as subspace estimation [25].

In order to define the moment function for the MTD, we first define the i-th observation from the signal y as follow:

$$y_i := [y[i], \ldots, y[i + L]]. \tag{19}$$

The moment function $f(\cdot)$ should fulfil (18) using the defined samples. The natural choice of $f(\cdot)$ is

$$f(x, \gamma, y_i) := \begin{bmatrix} \gamma A_x^1 - A_{y_i}^1 \\ \mathcal{A}_x^2 - \mathcal{A}_{y_i}^2 \\ \mathcal{A}_x^3 - \mathcal{A}_{y_i}^3 \end{bmatrix} \tag{20}$$

The estimated sample moment function is the average of f over N observations:

$$g_N(\theta) = \frac{1}{N}\sum_{i=1}^{N} f(\theta, y_i) = \begin{bmatrix} \gamma A_x^1 - A_y^1 \\ \mathcal{A}_x^2 - \mathcal{A}_y^2 \\ \mathcal{A}_x^3 - \mathcal{A}_y^3 \end{bmatrix}. \tag{21}$$

The GMM estimator is defined as the minimizer of the weighted LS expression,

$$\hat{\theta}_N = \arg\min_{\theta\in\Theta} \; g_N(\theta)^T W_N g_N(\theta). \tag{22}$$

Here, W_N is a fixed positive semi-definite (PSD) matrix. Note that the LS estimator (17) is a special case of (22).

3.2. Large Sample Properties

Before presenting the statistical properties of the GMM, we fix notation. We denote by $\xrightarrow{p}$ and $\xrightarrow{d}$ convergence in probability and in distribution, respectively. Let

$$S := \lim_{N\to\infty} \mathrm{Cov}\left[\sqrt{N} g_N(\theta_0)\right], \tag{23}$$

be the covariance matrix of the estimated sample moment function (21) at the ground truth θ_0. We denote by $\{W_N\}_{N=1}^{\infty}$

a sequence of PSD matrices which converges almost surely to a positive definite (PD) matrix W. Finally, the expectation of the Jacobian of the moment function at the ground truth θ_0 is denoted by $G_0 = \mathbb{E}\left[\partial f(\theta_0, y)/\partial \theta^T\right]$.

The large sample properties of the GMM estimator, were derived in [23], and are presented in the following theorem. The regularity conditions for this theorem can be found in many papers [23, 28, 24]

Theorem 3.1. *Under the regularity conditions, the GMM estimator satisfies:*

A. (Consistency) $\hat{\theta}_N \xrightarrow{p} \theta_0$.

B. (Asymptotic normality)

$$\sqrt{N}(\hat{\theta}_N - \theta_0) \xrightarrow{d} \mathcal{N}(0, MSM^T),$$

where $M = [G_0^T W G_0]^{-1} G_0^T W$.

C. (Optimal choice of a weighting matrix) *The minimum asymptotic variance of* $\hat{\theta}_N$ *is given by* $(G_0^T S^{-1} G_0)^{-1}$ *and is attained by* $W = S^{-1}$.

Theorem 3.1 provides a matrix W that guarantees a minimal asymptotic variance of the estimator's error.

The covariance matrix S of (23), which plays a central role in Theorem 3.1, is required to be a PD matrix. Therefore, the moment function must be chosen so that S is full-rank. As in [24], we remove the repeating entries of f (that appear due to the inherent symmetries of the autocorrelations).

It is important to note that in practice, the ground truth θ_0 is unknown a priori, so we cannot use the optimal weighting matrix. However, for our choice of the moment function (20), it is enough to apply the covariance on the empirical part,

$$\mathrm{Cov}[g(\theta)] = \mathrm{Cov}\left[\left[A^1_{y_i}; \mathcal{A}^2_{y_i}; \mathcal{A}^3_{y_i}\right]\right]. \tag{24}$$

The covariance depends solely on the observations $\{y_i\}_{i=1}^N$, and not on the parameter set θ.

4. NUMERICAL EXPERIMENTS

4.1. Experimental setting

In our numerical research of the GMM estimator, we implemented the numerical framework for signals estimation. For different SNR and signal's length N, we conducted 10 trails. In each trail, we drawn the signal $x \in \mathbb{R}^L$, where $L = 5$, from a normal distribution, and then normalized it such that $|x|_2 = 1$. The density variable γ is sampled uniformly between $[0, 0.3]$ we compared between the GMM and MoM estimations error using the L_2-norm. The signal y is generated according to (1).

We apply the estimator as described in previous section, and the optimization was solved via interior-point algorithm, which was implemented in Scipy.[Asaf: I didn't make sure if those are the setting and just put the structure itself]

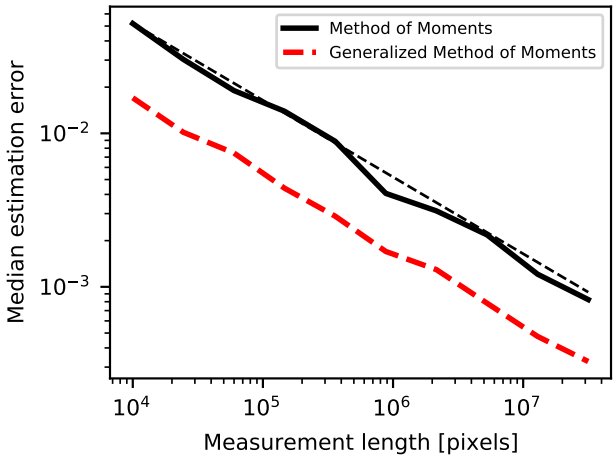

Fig. 2: Median estimation error of recovering the signal x, as a function of the measurement size, by: (a) the method of moments; (b) the generalized method of moments. [Asaf: We need to fix the x-axis to: N - signal's length. In general we should make the dashed red on to not dashed and explain what is the black dashed one]

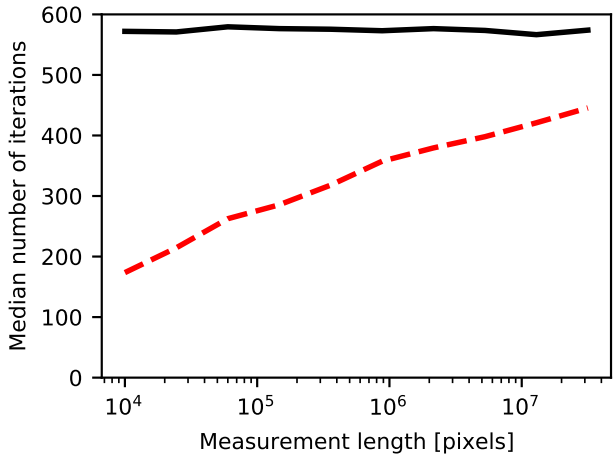

Fig. 3: Median number of optimization iterations in recovering the signal x, as a function of the measurement size, by: (a) the method of moments; (b) the generalized method of moments. [Asaf: I am not sure that this one is relevant]

4.2. Numerical validation of the convergence rate

From the law of large numbers it is known that both estimators' errors decay as $N^{-0.5}$. In addition, Theorem 3.1 provides the optimality of the GMM estimator, over the MoM estimator. Both properties can be observed in Figure 2.

5. CONCLUSION

6. REFERENCES

[1] Tamir Bendory, Nicolas Boumal, William Leeb, Eitan Levin, and Amit Singer, "Multi-target detection with application to cryo-electron microscopy," *Inverse Problems*, vol. 35, no. 10, pp. 104003, 2019.

[2] Ti-Yen Lan, Tamir Bendory, Nicolas Boumal, and Amit Singer, "Multi-target detection with an arbitrary spacing distribution," *IEEE Transactions on Signal Processing*, vol. 68, pp. 1589–1601, 2020.

[3] Nicholas F Marshall, Ti-Yen Lan, Tamir Bendory, and Amit Singer, "Image recovery from rotational and translational invariants," in *ICASSP 2020-2020 IEEE International Conference on Acoustics, Speech and Signal Processing (ICASSP)*. IEEE, 2020, pp. 5780–5784.

[4] Tamir Bendory, Ti-Yen Lan, Nicholas F Marshall, Iris Rukshin, and Amit Singer, "Multi-target detection with rotations," *arXiv preprint arXiv:2101.07709*, 2021.

[5] Shay Kreymer and Tamir Bendory, "Two-dimensional multi-target detection," *arXiv preprint arXiv:2105.06765*, 2021.

[6] Tamir Bendory, Nicolas Boumal, William Leeb, Eitan Levin, and Amit Singer, "Toward single particle reconstruction without particle picking: breaking the detection limit," *arXiv preprint arXiv:1810.00226*, 2018.

[7] Sandeep Gogineni, Pawan Setlur, Muralidhar Rangaswamy, and Raj Rao Nadakuditi, "Passive radar detection with noisy reference channel using principal subspace similarity," *IEEE Transactions on Aerospace and Electronic Systems*, vol. 54, no. 1, pp. 18–36, 2017.

[8] Timothy J Schulz, "Multiframe blind deconvolution of astronomical images," *JOSA A*, vol. 10, no. 5, pp. 1064–1073, 1993.

[9] Anat Levin, "Blind motion deblurring using image statistics," *Advances in Neural Information Processing Systems*, vol. 19, pp. 841–848, 2006.

[10] Karim Abed-Meraim, Wanzhi Qiu, and Yingbo Hua, "Blind system identification," *Proceedings of the IEEE*, vol. 85, no. 8, pp. 1310–1322, 1997.

[11] Richard Henderson, "The potential and limitations of neutrons, electrons and X-rays for atomic resolution microscopy of unstained biological molecules," *Quarterly Reviews of Biophysics*, vol. 28, no. 2, pp. 171–193, 1995.

[12] Eva Nogales, "The development of cryo-EM into a mainstream structural biology technique," *Nature methods*, vol. 13, no. 1, pp. 24–27, 2016.

[13] Xiao-Chen Bai, Greg McMullan, and Sjors HW Scheres, "How cryo-EM is revolutionizing structural biology," *Trends in Biochemical Sciences*, vol. 40, no. 1, pp. 49–57, 2015.

[14] Joachim Frank, *Three-dimensional electron microscopy of macromolecular assemblies: visualization of biological molecules in their native state*, Oxford University Press, 2006.

[15] Ayelet Heimowitz, Joakim Andén, and Amit Singer, "Reducing bias and variance for CTF estimation in single particle cryo-EM," *Ultramicroscopy*, vol. 212, pp. 112950, 2020.

[16] HP Erickson and Aaron Klug, "Measurement and compensation of defocusing and aberrations by Fourier processing of electron micrographs," *Philosophical Transactions of the Royal Society of London. B, Biological Sciences*, vol. 261, no. 837, pp. 105–118, 1971.

[17] Tamir Bendory, Alberto Bartesaghi, and Amit Singer, "Single-particle cryo-electron microscopy: Mathematical theory, computational challenges, and opportunities," *IEEE Signal Processing Magazine*, vol. 37, no. 2, pp. 58–76, 2020.

[18] Sjors HW Scheres, "RELION: implementation of a Bayesian approach to cryo-EM structure determination," *Journal of Structural Biology*, vol. 180, no. 3, pp. 519–530, 2012.

[19] Ali Punjani, John L Rubinstein, David J Fleet, and Marcus A Brubaker, "cryoSPARC: algorithms for rapid unsupervised cryo-EM structure determination," *Nature methods*, vol. 14, no. 3, pp. 290–296, 2017.

[20] Cecilia Aguerrebere, Mauricio Delbracio, Alberto Bartesaghi, and Guillermo Sapiro, "Fundamental limits in multi-image alignment," *IEEE Transactions on Signal Processing*, vol. 64, no. 21, pp. 5707–5722, 2016.

[21] Edoardo D'Imprima and Werner Kühlbrandt, "Current limitations to high-resolution structure determination by single-particle cryoEM," *Quarterly Reviews of Biophysics*, vol. 54, 2021.

[22] Karl Pearson, "Contributions to the mathematical theory of evolution," *Philosophical Transactions of the Royal Society of London. A*, vol. 185, pp. 71–110, 1894.

[23] Lars Peter Hansen, "Large sample properties of generalized method of moments estimators," *Econometrica*, vol. 50, no. 4, pp. 1029, 1982.

[24] Asaf Abas, Tamir Bendory, and Nir Sharon, "The generalized method of moments for multi-reference alignment," 2021.

[25] Jianqing Fan and Yiqiao Zhong, "Optimal subspace estimation using overidentifying vectors via generalized method of moments," *arXiv preprint arXiv:1805.02826*, 2018.

[26] David Roodman, "How to do xtabond2: An introduction to difference and system GMM in stata," *The stata journal*, vol. 9, no. 1, pp. 86–136, 2009.

[27] Nicolas Boumal, Tamir Bendory, Roy R. Lederman, and Amit Singer, "Heterogeneous multireference alignment: A single pass approach," in *2018 52nd Annual Conference on Information Sciences and Systems (CISS)*, 2018, pp. 1–6.

[28] Alastair R Hall, *Generalized method of moments*, Oxford university press, 2005.